J Neurophysiol 115: 2705–2720, 2016.
First published December 9, 2015; doi:10.1152/jn.00639.2014.

Properties of pattern and component direction-selective cells in area MT of the macaque

Helena X. Wang and J. Anthony Movshon
Center for Neural Science, New York University, New York, New York

Submitted 26 August 2014; accepted in final form 9 November 2015

Wang HX, Movshon JA. Properties of pattern and component direction-selective cells in area MT of the macaque. *J Neurophysiol* 115: 2705–2720, 2016. First published December 9, 2015; doi:10.1152/jn.00639.2014.—Neurons in area MT/V5 of the macaque visual cortex encode visual motion. Some cells are selective for the motion of oriented features (component direction-selective, CDS); others respond to the true direction of complex patterns (pattern-direction selective, PDS). There is a continuum of selectivity in MT, with CDS cells at one extreme and PDS cells at the other; we compute a pattern index that captures this variation. It is unknown how a neuron's pattern index is related to its other tuning characteristics. We therefore analyzed the responses of 792 MT cells recorded in the course of other experiments from opiate-anesthetized macaque monkeys, as a function of the direction, spatial frequency, drift rate, size, and contrast of sinusoidal gratings and of the direction and speed of random-dot textures. We also compared MT responses to those of 718 V1 cells. As expected, MT cells with higher pattern index tended to have stronger direction selectivity and broader direction tuning to gratings, and they responded better to plaids than to gratings. Strongly PDS cells also tended to have smaller receptive fields and stronger surround suppression. Interestingly, they also responded preferentially to higher drift rates and higher speeds of moving dots. The spatial frequency preferences of PDS cells depended strongly on their preferred temporal frequencies, whereas these preferences were independent in component-selective cells. Pattern direction selectivity is statistically associated with many response properties of MT cells but not strongly associated with any particular property. Pattern-selective signals are thus available in association with most other signals exported by MT.

extrastriate visual cortex; macaques; visual motion processing; neural dynamics; receptive fields

THE ANALYSIS OF COMPLEX OBJECT MOTION requires the integration of local motion signals over contour orientation and spatial position. A direction-selective V1 cell functions like a local motion detector, in that it can only selectively respond to the velocity of a local oriented feature. To compute the velocity of a more complex pattern, the brain must pool information from many local detectors. In primates, cortical area MT is a candidate area for such computation. Cells in MT are selective for the direction of motion and pool inputs from direction-selective cells in V1 (Dubner and Zeki 1971; Movshon and Newsome 1986). Measurement of responses to coherently moving plaid stimuli, made up of two sinusoidal gratings of different orientations, provides a way to quantify the degree of selectivity to pattern motion. Some MT cells, like their V1 afferents, respond only to the direction of motion of the component gratings. Others, however, are able to signal the true direction of the pattern by integrating motion information of its constituent components (Khawaja et al. 2009; Movshon et al. 1985; Nishimoto and Gallant 2011; Rodman and Albright 1989; Rust et al. 2006; Smith et al. 2005; Stoner and Albright 1992).

There is a continuum of pattern selectivity in MT, with the two canonical types at the extremes. The range is captured by a pattern index, in which component direction-selective (CDS) cells have negative values and pattern direction-selective (PDS) cells have positive ones. We wondered whether pattern selectivity was associated with other kinds of stimulus selectivity found in MT cells. We therefore analyzed the properties of a population of 792 MT cells recorded from 58 opiate-anesthetized, paralyzed macaque monkeys. We examined how responses depended on the direction, spatial frequency, temporal frequency, target size, and contrast of drifting sinusoidal gratings, as well as on the direction and speed of coherently moving random-dot textures. We analyzed the association of each of these properties with pattern selectivity. Because MT responses are derived in large part from V1 inputs (Movshon and Newsome 1996; Rodman et al. 1989), we measured corresponding properties for a population of 718 V1 cells to gain an overview of the transformation that takes place between V1 and MT.

The pattern index is statistically associated with many properties of MT cells. Pattern-selective cells tended to have stronger direction selectivity and broader direction tuning to gratings, and they responded better to plaids than to gratings. Cells that were more pattern selective also tended to have smaller receptive fields and to show stronger surround suppression. These findings are consistent with a model for the mechanism of pattern selectivity that depends on the pooling of V1 inputs with a wide range of spatiotemporal selectivities (Rust et al., 2006). We also found relationships between pattern selectivity and temporal dynamics. Cells that were pattern selective tended to respond preferentially to higher temporal frequencies of drift and were also tuned to higher speeds of moving dots. These results are not predicted by known or hypothesized mechanisms of pattern selectivity and may reflect differences in the circuitry or processing dynamics of cells with the two kinds of selectivity. The significance of these relationships for motion integration is an interesting avenue for further exploration.

MATERIALS AND METHODS

Electrophysiology

Data were taken from MT cells recorded in our laboratory between 1998 and 2008. Altogether, we analyzed units recorded from 58 adult

Address for reprint requests and other correspondence: J. A. Movshon, Center for Neural Science, New York Univ., 4 Washington Place, Rm 809, New York, NY 10003 (e-mail: movshon@nyu.edu).

monkeys (49 male, 9 female), including 38 cynomolgus (*Macaca fascicularis*), 18 pig-tailed (*M. nemestrina*), and 2 bonnet (*M. radiata*) macaques. A comparison set of V1 data was that collected and published by Cavanaugh et al. (2002a, 2002b). These units came from 25 adult monkeys (21 male, 4 female), including 13 cynomolgus and 12 pig-tailed macaques. Details of the surgical preparation were as detailed previously (Cavanaugh et al. 2002a; Smith et al. 2005). Anesthesia (sufentinil citrate, 4–30 $\mu g \cdot kg^{-1} \cdot h^{-1}$) and neuromuscular blockade (vecuronium bromide, or Norcuron, 0.15 $\mu g \cdot kg^{-1} \cdot h^{-1}$) were maintained for the duration of each experiment. MT single neurons were identified, isolated, and recorded using standard procedures of our laboratory (Cavanaugh et al. 2002a). At the end of most experiments, confirmation that recording sites lay within MT was established with histological identification (Nissl- or myelin-stained frozen sections) of electrolytic lesions made with the electrode tip; in other cases we relied on the physiological properties and recording depth of the neurons to identify them as lying in MT. We did not consistently reconstruct the laminar location of recorded neurons. All procedures complied with guidelines approved by the New York University Animal Welfare Committee.

Stimuli

For all experiments analyzed in the current study, stimuli were displayed on a gamma-corrected CRT monitor (Eizo T550 or Eizo T966) located 60–180 cm from the eyes, subtending 10°–30° of visual angle. The monitor was refreshed at 100 or 120 Hz and had a horizontal resolution in excess of 1,000 pixels with a mean luminance of 33 cd/m^2. Each stimulus was displayed within a circular aperture surrounded by a mean luminance gray field. The eye through which stronger responses were evoked was chosen as the dominant eye, and all stimuli were presented to that eye with the other eye covered. Receptive field eccentricity estimates (available for most cells) were derived from maps made by hand; 90% of the cells had receptive fields within 18° of the center of gaze.

In this article we describe analyses of a number of different measurements, not all of which were made on all neurons. For most neurons, measurements were made of the optimal direction of motion, spatial frequency, temporal drift rate, and stimulus size for a high-contrast drifting sinusoidal grating. For a smaller subset of the cells, the contrast response function was also obtained by varying the luminance contrast of an otherwise optimal grating stimulus. The experiments were typically conducted in the order mentioned. In spatial frequency tuning experiments, sinusoidal gratings drifted at a fixed rate in the preferred direction of the cell while their spatial frequencies varied in octave steps. Tuning drift rate was measured, in octave or half-octave steps (typically 0.2–25 Hz), using gratings at the cell's preferred spatial frequency. Spatial frequency tuning was sometimes remeasured if the optimal drift rate was determined to be substantially different from the drift rate used for the initial spatial frequency tuning measurement. Stimuli shown thereafter were at the optimal spatial frequency and drift rate confined to the cell's classical receptive field (Cavanaugh et al. 2002a).

A dynamic random sequence of plaids and gratings was used to probe the pattern selectivity of each cell (Smith et al. 2005). During each interval, the stimulus was either a 50%-contrast grating moving in 1 of 12 directions or a plaid constructed by adding two such gratings oriented 120° apart. Four equivalent periods of blank screen were inserted to measure spontaneous activity.

For a subset of the cells (24%; see Table 1), responses to random-dot textures were also measured. A dot texture consisted of randomly positioned bright dots, size typically 0.04° and density typically at 100–200 dots$\cdot$deg$^{-2}\cdot$s^{-1}. All dot textures were presented within a circular aperture. Direction tuning experiments consisted of dot textures translating coherently in 1 of 12, 16, or 24 directions. Speed tuning was also obtained for some of these cells for dot textures moving coherently in the preferred dot direction. Baseline activity for dot stimuli was taken from interleaved presentations of zero-coherence dynamic random dots.

All stimuli were shown using one of two types of presentation protocols. Under the first protocol, within each experimental block, stimuli of equal duration (typically 1.2–5 s) were separated by the presentation of a mean luminance gray background for about 1.5 s. Each experiment typically consisted of 2–10 such blocks of trials; those with fewer than 2 trials for each stimulus were excluded from analysis. Under the second protocol, stimuli were presented in a continuous stream, typically for 320 ms at a time, and followed by one another in rapid succession. Each stimulus typically had 25–300 presentations. Latency was recovered by choosing the time that maximized the modulation of the tuning curve, or the variance across all presented stimulus values, as described in detail by Smith et al. (2005). Fifty-five percent of analyzed experiments followed this second protocol. Both types of experiments always included trials with a uniform gray field stimulus of the same duration to measure spontaneous activity. For each experiment, all stimuli were randomly interleaved, and the mean response was obtained by averaging over repeated measurements for each stimulus value.

Model Fitting and Assessing the Goodness of Fit

We analyzed neuronal responses from separate experiments (spatial frequency, temporal drift rate, size, contrast, direction and speed of dot textures) in relation to pattern direction selectivity of each MT cell. We fit the available tuning responses of each neuron to idealized tuning curves by minimizing the negative log-likelihood error between measured and predicted responses, computed as follows.

The model provided an estimate of the mean firing rate. We assumed that the empirically observed spike count was Poisson distributed and that the mean of that distribution depended on the model prediction. It follows that, for a given stimulus, the likelihood of the data given the model can be written as $e^o \exp(-e)/o!$, where o is the observed total spike count (across passes and stimulus duration) and e is the model spike count (converted from the model rate). The likelihood of the data for a given experiment is the product of likelihoods for all individual stimulus values. Finally, a log transform is applied for computational convenience. Thus the log-likelihood of the data for a given model can be expressed as

$$L(e;o) = \sum_i o_i \log(e_i) - (e_i) - \log(o_i!), \qquad (1)$$

where o_i is the total spike count for the ith stimulus and e_i is the spike count predicted by the model. For each experiment, we found the set of parameters for the model that best predicted the data by minimizing $-L$ (i.e., maximizing the likelihood) using the constrained nonlinear minimization tool (*fmincon* function) in MATLAB (The MathWorks, Natick, MA). We used a multi-start procedure with 10–30 sets of different initial values to find the most probable global minimum for each fit. In all cases, any negative values determined by the fit were set to zero so that response amplitude was nonnegative.

The functions used to fit each type of response and the descriptions for their parameters are described in detail in the following section and summarized in Table 1. To assess the goodness of a fit, we computed the normalized log-likelihood (*NLL*), which allowed us to make comparisons across different tuning functions with varying numbers of model parameters. Specifically, we computed the log-likelihoods of spike rate predictions provided by a "null model" (L_{Null}) and that by a "saturated model" (L_{Sat}), which served as the lower and upper bounds, respectively, for the log-likelihood of the best fit (L). For the null model, the predicted response at all stimulus values was the mean firing rate measured across all non-blank conditions (i.e., the DC response). For the saturated model, the predicted firing rate at each stimulus value was equal to the empirically measured mean rate (i.e., no residual error between empirical data and model predictions). In each case, firing rate predictions were con-

Table 1. *Equations and statistics used to derive parameters of interest from neuronal tuning curves*

Tuning Data Type	Equation	Free Parameters	Extracted Measures	Total No. Cells (No. Excluded)	Median *NLL*
Direction (gratings)	$r(\theta) = \exp\left[\frac{\cos(\theta-\theta_p)}{w}\right] + a_n \exp\left[\frac{\cos(\theta-\theta_p-\pi)}{w}\right]$	R_0 = baseline response A_p = amplitude in preferred direction		835 (43)	0.92
Direction (dots)	$R(\theta) = R_0 + A\{r(\theta) - min[r(\theta)]\}$	a_n = relative amplitude in null direction θ_p = preferred direction w = circular Gaussian width	Bandwidth	192 (6)	0.93
Spatial frequency (gratings)	$R(s) = R_0 + A \exp\left[\frac{-\log\left(\frac{s+s_0}{s_p+s_0}\right)^2}{2\sigma^2}\right]$	R_0 = baseline response A = amplitude s_p = optimal frequency/speed σ = log-Gaussian width s_0 = offset	Optimal SF, Bandwidth	701 (16)	0.93
Speed (dots)			Optimal speed	89 (3)	0.89
Drift rate (gratings)			Optimal drift rate, High-pass index	703 (4)	0.94
Stimulus diameter (gratings)	$R(x) = R_0 + \frac{A_c\left[erf\left(\frac{x}{w_c}\right)\right]^2}{1+A_s\left[erf\left(\frac{x}{w_s}\right)\right]^2}$ (erf denotes the error function)	R_0 = baseline response A_c = amplitude of center component A_s = amplitude of surround component w_c = width of center component w_s = width of surround component	$SIZE_{75}$, Suppression index	587 (17)	0.96
Contrast response (gratings)	$R(c) = R_0 + A\frac{c^n}{c^n+\beta^n}$	R_0 = baseline response A = amplitude n = exponent β = semisaturation contrast	c_{50}, Slope at c_{50}	376 (8)	0.94

NLL, normalized log-likelihood; SF, spatial frequency; erf, error function; $SIZE_{75}$, receptive field size; c_{50}, 50% contrast response.

verted into spike counts to compute L_{Null} and L_{Sat} using *Eq. 1*. We normalized the log-likelihood value of the best fitting functional model by L_{Null} and L_{Sat}, or $NLL = (L - L_{Null})/(L_{Sat} - L_{Null})$. This indicated the relative distance of L to its upper and lower bounds; a value close to 1 indicated a good fit, and a value near or less than 0 indicated a poor fit. Overall, the tuning functions described the data well, yielding high values of *NLL* for most of tuning responses under study (see Table 1, *Median NLL*).

Tuning Functions for Model Fitting and Parameters of Interest

Motion direction tuning. Direction tuning responses for gratings and for dots were fit with a doubled von Mises function, the sum of two circular Gaussians:

$$r(\theta) = \exp\left[\frac{\cos(\theta - \theta_p)}{w}\right] + a_n \exp\left[\frac{\cos(\theta - \theta_p - \pi)}{w}\right], \quad (2)$$
$$R(\theta) = R_0 + A\{r(\theta) - \min[r(\theta)]\}$$

where θ denotes the stimulus direction of motion and R_0, A, a_n, θ_p, and w are free parameters. The two exponentials in the expression $r(\theta)$ correspond to two circular Gaussian peaks centered at θ_p and $\theta_p + \pi$ (preferred and opposite directions, respectively) with width w (same for both Gaussians). The parameter a_n scales the height of the peak in the opposite direction relative to that in the preferred direction (constrained to be between 0 and 1 during the fit); A scales the overall amplitude of the fitted response. R_0 captures the baseline response. We subtracted $r(\theta)$ by its minimum value during the fit, because as w increases, $r(\theta)$ tends to shift vertically above 0; subtracting $\min[r(\theta)]$ before adding in R_0 therefore ensured that R_0 alone captured the elevation of the curve above 0. We determined a bandwidth measure from each fitted tuning curve, defined as the full width (in degrees of polar angle) at half-maximal height of the fitted, baseline-subtracted response. Note that the baseline used in estimating bandwidth was R_0, which by design bounds bandwidth above by 180°. Parameter w was constrained during the fitting such that the derived bandwidth was bound below by the minimum spacing (in polar angles) between directions of motion of adjacent stimuli (30° for gratings and 15°, 22.5°, or 30° for dots, depending on the experiment).

Spatial frequency, drift rate, and speed tuning. We fit the spatial frequency responses with a log-Gaussian function (Nover et al. 2005):

$$R(s) = R_0 + A \exp\left[\frac{-\log\left(\frac{s + s_0}{s_p + s_0}\right)^2}{2\sigma^2}\right], \quad (3)$$

where s denotes the spatial frequency in cycles/deg and R_0, A, s_p, s_0, and σ are free parameters. The parameter s_p controls the optimal spatial frequency. Parameter σ determines the width of the tuning curve (in log units). A and R_0 capture the maximal and baseline response amplitudes, respectively. The parameter s_0 is an offset that keeps the logarithm from being undefined.

We defined the parameter s_p obtained from the best fitting function to be the optimal spatial frequency for the cell (in cycles/deg). Some cells showed responses that did not attenuate below maximum at either the lowest or highest spatial frequency presented; we therefore could not reliably determine the true optimal spatial frequency from those fits. Those cells were excluded from the analyses involving spatial frequency and were treated separately. This constituted 58/685 cells (42 low-pass cells and 16 high-pass cells).

We also estimated the bandwidth of each spatial frequency response function by calculating the fitted response (using the best-fitting parameters) for spatial frequencies ranging from half of the lowest presented stimulus value to 1.5 times the highest presented stimulus value. Bandwidth is the width (in log units) at half-maximal height of the fitted, baseline-subtracted response and is undefined for cells with fitted responses that did not drop by half on either side of the tuning curve (187/685 cells).

The same log-Gaussian function was also used to fit tuning responses for temporal drift rate of gratings and for motion speed of dot textures. For each of those fitted response functions, we obtained the optimal drift rate (in Hz) or optimal speed (in deg/s) in a manner analogous to that for optimal spatial frequency above. There were 39/699 cells for which the optimal drift rate could not be obtained (2

low-pass cells and 37 high-pass cells) because of the lack of attenuation in response. There were 7/86 cells for which the optimal speed could not be obtained (5 low-pass cells and 2 high-pass cells).

We also quantified the shape of drift rate tuning function with a "temporal high-pass index," or the slope of the fitted tuning curve along the low-frequency limb (Levitt et al. 2001). This was defined as $(R_{opt} - R_{1/4f})/R_{opt}$, where R_{opt} was the maximal response (at the preferred drift rate) and $R_{1/4f}$ was the response at one-fourth of the preferred drift rate. Both R_{opt} and $R_{1/4f}$ were baseline subtracted.

Optimal stimulus diameter. Responses for varying diameters of grating patches were fit with a ratio-of-Gaussians function (Cavanaugh et al. 2002a):

$$R(x) = R_0 + \frac{A_c\left[\mathrm{erf}\left(\frac{x}{w_c}\right)\right]^2}{1 + A_s\left[\mathrm{erf}\left(\frac{x}{w_s}\right)\right]^2}, \quad (4)$$

where x is the grating stimulus diameter (in degrees of visual angle), and erf denotes the error function. R_0, A_c, A_s, w_c, and w_s are free parameters. A_c and w_c (A_s and w_s) determine the gain and the spatial width of the center (surround) component, respectively. We constrained $w_c < w_s$ during the fit.

From each fit we determined a $SIZE_{75}$ measure and a suppression index (SI). $SIZE_{75}$ corresponded to the point at which the cell reached at least 75% of its maximal response on the rising side of the tuning function. Whereas 95% is commonly used as a criterion for determining the optimal stimulus diameter (e.g., in V1; Cavanaugh et al. 2002a), many neurons in our MT population preferred large stimulus sizes, thereby approaching saturation only near the largest stimulus diameter possible for the display. The 75% criterion yielded a more reliable measure of diameter preferences because it derived from a more sensitive region of the curve, whereas the 95% criterion was more affected by experimental display limits. Fits that resulted in accelerating tuning responses did not yield meaningful $SIZE_{75}$ measures; we therefore specified $SIZE_{75}$ as undefined for cells that had a fitted response at the largest stimulus diameter that was convex (positive 2nd derivative). There were 19/570 such cells.

SI indicated the strength of surround suppression shown by a cell. It was defined as the relative reduction from the fitted maximal response to the asymptotic, suppressed response with an increasingly larger stimulus diameter (Cavanaugh et al. 2002a), or $SI = 1 - R_{supp}/R_{opt}$, where R_{supp} is the final, suppressed response at the largest grating diameter and R_{opt} is the maximal response.

Contrast response functions. Finally, contrast responses were fit with a hyperbolic ratio function (Albrecht and Hamilton 1982; Naka and Rushton 1966):

$$R(c) = R_0 + A\frac{c^n}{c^n + \beta^n}, \quad (5)$$

where c denotes the luminance contrast of the grating stimulus, and R_0, A, n, and β are free parameters. A and R_0 capture the maximal and baseline responses, respectively. Parameters β and n control the contrast and rate at which the curve rises. We constrained β to be between 0 and 1 and n to be between 0.01 and 8 during the fit. We determined a c_{50} value from each fitted response, defined as the contrast needed to reach at least half of the fitted response at the highest contrast. Note that this value is similar to that given by the best-fitting parameter β but is less sensitive to fit error and better captures the shape of the curve, particularly in cases in which R does not saturate at maximal contrast. Additionally, we determined a slope measure from each fit, corresponding to the slope of R in the vicinity of c_{50} (± 0.1 log contrast units).

Other parameters of interest. In addition, we estimated the direction selectivity of each cell directly from the responses to drifting gratings. This was quantified using a directionality index (DI), or $DI = 1 - R_n/R_{opt}$, where R_{opt} was the measured maximal response of the cell (at the preferred direction of motion) and R_n was the response 180° away (at the null direction). Both R_n and R_{opt} were baseline subtracted. Two cells were excluded because the measured spontaneous rate was higher than the maximal response.

We also quantified orientation selectivity (orientation selectivity index, or OSI) from the responses to drifting gratings with a vector-based measure of tuning strength. The response of the cell to a grating of a particular orientation corresponded to a vector with its polar angle equal to the orientation of the grating and its magnitude equal to the firing rate. OSI was computed as the summed response vector (over the orientation range 0°–180°), normalized by the summed magnitude across all response vectors (see Smith et al. 2002 for details).

Correlation Analysis

We used the Pearson's product-moment correlation coefficient r to assess the relationship between two measures X and Y (e.g., between pattern index and grating tuning bandwidth). For all figures in which a scatter plot between two measures X and Y is shown, we superimpose the 95% covariance ellipse, stretched roughly 2 standard deviations along the principal components of the data points, determined by the covariance $E[(X - \mu_X)(Y - \mu_Y)]$, to illustrate the strength and direction of the correlation between X and Y. In each case, to assess whether r was significantly different from zero, we randomly permuted the entries in X and recomputed the correlation coefficient between X and Y. This procedure was carried out 5,000 times to yield a null distribution for r between X and Y. We defined the P value as the fraction of the null distribution that was as large or larger than the correlation observed without randomization.

As noted above, cells were tested using two protocols, one using discrete trials and one using continuous stimulation. Analyses performed separately for data obtained using the two protocols for the most part yielded qualitatively and quantitatively similar results as for the combined data (Table 2) and supported the same conclusions; two exceptions are discussed below. For subsequent analysis, we pooled data acquired using the two protocols.

V1 Sample

We compared the distributions of neuronal measures in MT cells to comparable measures in a population of 718 V1 cells collected and quantified by Cavanaugh et al. (2002a, 2002b). The fits used to characterize the responses of V1 cells and the measures extracted from theses fits are as detailed in Cavanaugh et al. (2002a, 2002b). In those experiments, the receptive field diameter for V1 was taken as the stimulus diameter that elicited 95% of the maximal response. To determine a criterion diameter comparable to the $SIZE_{75}$ measure we calculate for MT cells, we made the simplifying assumption that area summation curves are roughly linear with stimulus size for V1 (cf. data in Cavanaugh et al. 2002a). The appropriate comparison with MT was therefore computed by multiplying the 95% diameter by 75/95 to calculate a $SIZE_{75}$ measure for V1 cells. Overall, our V1 sample included 677 cells for measures of grating direction selectivity, 655 cells for spatial frequency tuning, 628 cells for drift rate tuning, and 585 cells for stimulus diameter tuning.

MT Sample

We started with an initial sample of 841 MT neurons. Because most of our analyses concerned relationships with pattern direction selectivity, we excluded from the overall sample those cells for which pattern index was likely to be unreliable. This was done based on two criteria: poor fit and poor tuning. We first excluded cells that yielded low *NLL* (<0.5) for the fits to grating direction tuning. Note that although pattern index was computed from the grating and plaid response measurements (rather than the fit), in practice *NLL* for the

Table 2. *Comparison of correlations between pattern index and other derived metrics*

Metric	Discrete Trial Protocol			Continuous Protocol			Combined			*r*-Value Difference
	r	*N*	*P*	*r*	*N*	*P*	*r*	*N*	*P*	*P*
Directionality index	0.28	184	0.000	0.24	599	0.000	0.25	783	0.000	0.6132
Grating direction bandwidth	0.33	187	0.000	0.36	605	0.000	0.35	792	0.000	0.6860
Dot direction bandwidth	−0.18	70	0.070	0.03	116	0.376	−0.05	186	0.242	0.1692
Optimal spatial frequency	0.09	279	0.060	−0.19	348	0.000	−0.07	627	0.032	**0.0005**
Spatial frequency bandwidth	0.02	207	0.374	−0.01	291	0.436	0.00	498	0.488	0.7430
Receptive field size ($SIZE_{75}$)	−0.18	392	0.000	−0.03	159	0.364	−0.11	551	0.007	0.1088
Suppression index	0.15	263	0.007	0.02	138	0.410	0.10	401	0.020	0.2164
Optimal drift rate	0.13	303	0.014	0.23	357	0.000	0.19	660	0.000	0.1874
Temporal highpass index	0.12	326	0.012	0.07	373	0.084	0.11	699	0.002	0.5075
Optimal dot speed	0.35	50	0.008	−0.13	29	0.263	0.20	79	0.033	0.0423
Contrast-response slope	−0.08	148	0.168	0.04	220	0.271	−0.01	368	0.442	0.2625
Contrast-response c_{50}	0.22	148	0.003	−0.14	220	0.019	−0.01	368	0.445	**0.0007**

Values are correlations between pattern index and 12 other derived metrics for data obtained using either discrete trials or continuous stimulus presentation. In 2 cases, the difference in correlation was significant ($P < 0.004$, Bonferroni corrected; indicated in bold type).

grating fits served as a good proxy for the quality of data, because most poor fits resulted from noisy and unreliable responses (due to low firing rate or poor unit isolation). We also excluded cells with untuned responses for grating directions because they did not yield meaningful pattern predictions (and hence pattern indexes). To assess the magnitude of tuning, for each cell and each experiment we computed the standard deviation of the mean firing rates across all stimulus values and normalized it by the maximum response. Cells with normalized standard deviations in the bottom 2.5% yielded little response modulation and were excluded. We excluded 43/841 cells on the basis of these criteria and 6 additional cells that were not selective for gratings and plaid motion. Overall, this yielded a sample of 792 units for further analyses. This sample included 179 PDS cells and 296 CDS cells. These proportions are comparable to those reported previously using similar stimuli (Priebe et al. 2003; Smith et al. 2005).

For analyses involving each type of tuning experiment, we further excluded cells (out of subsets of the possible 792 neurons) that had had poorly fit responses for the response measure under study ($NLL < 0.5$). We found that this criterion was conservative and excluded only a small proportion of cells that showed the noisiest responses. Overall, we excluded 6/701 cells for spatial frequency, 4/703 cells for drift rate, 17/587 cells for stimulus diameter, 8/376 cells for contrast response, 6/192 cells for dot direction, and 3/89 cells for dot speed (see Table 1 for summary).

Multivariate Analysis and Dimensionality Reduction

We used multiple regression and principal component analysis (PCA) to explore the relationships among nine spatial and temporal variables and their contributions to pattern index. Eccentricity was also included as a variable, not because we expected it to predict pattern index but because it covaried with some of the other variables and therefore might partially explain their contributions to pattern index. For these analyses, we first transformed the values for drift rate, spatial frequency, $SIZE_{75}$, c_{50}, and slope at c_{50} by taking their log, and those for eccentricity by adding 1 and then taking the log, such that the distributions of all response variables were approximately Gaussian. We then computed regression and PCA on the *Z* scores of all variables.

RESULTS

Our sample of 792 MT neurons was drawn from an initial set of 841 recorded from 58 anesthetized animals (see above). Units included in the analysis were selected on the basis of the availability of plaid direction tuning measurements, as well as at least one other measurement of a response property under study. For comparison, we also analyzed a sample of 718 V1 neurons recorded from 19 animals (Cavanaugh et al. 2002a, 2002b).

Neuronal Tuning Examples

The spatial and temporal selectivities of the neurons were determined for drifting sinusoidal gratings. For a small subset of the cells, direction and speed tuning profiles were measured for dot textures. We fit the available tuning responses of each neuron to a set of idealized tuning curves, using equations described above and in Table 1. Overall, these provided good fits to the tuning responses. Note that most of the neurons in our sample were tested on only a subset of all tuning measurements (Table 1). The responses of a representative neuron and the fits to those responses are illustrated in Fig. 1. We derived a set of characteristic measures from each fit, as indicated in Fig. 1.

The example neuron showed direction-selective responses to gratings (Fig. 1*A*) and to dots (Fig. 1*F*). We fit the direction tuning responses for gratings and for dots with a double von Mises (sum of circular Gaussians) function, from which we estimated the bandwidth, or the full width at half-maximal height of the fitted, baseline-subtracted response. For the example neuron, the direction bandwidth was broader for dots (162°) than for gratings (106°).

We fit the tuning responses for spatial frequency and drift rate of gratings as well as for speed of dots with a log-Gaussian function (Nover et al. 2005) and extracted the optimal spatial frequency (Fig. 1*B*), optimal drift rate (Fig. 1*D*), and optimal speed (Fig. 1*G*), respectively. The example neuron showed band-pass spatial frequency tuning with an optimal spatial frequency at 1.2 cycles/deg (Fig. 1*B*), high-pass temporal frequency tuning with an optimal drift rate at 20.2 Hz (Fig. 1*D*), and band-pass speed tuning for dots with an optimal speed at 22.1 deg/s (Fig. 1*G*). For the spatial frequency response function, we also estimated the bandwidth of spatial frequency tuning as the width (in octaves) at half-maximal height of the fitted, baseline-subtracted response (Fig. 1*B*). The example cell had a spatial frequency bandwidth of 1.9 octaves. For the temporal frequency response function, we also estimated a "temporal high-pass index" (Fig. 1*D*), the slope of the fitted tuning curve along its low-frequency limb (Levitt et al. 2001). The high-pass index indicates the transience of the cell's inferred step response in the time domain: a cell with a

high-pass index near 0 corresponded to a low-pass drift rate tuning function and presumably more sustained response dynamics to a step stimulus presentation (assuming linear temporal summation). Conversely, a cell with a large high-pass index had greater attenuation of responses to low drift rates (more band-pass behavior) and presumably more transient response dynamics. The example cell had a high-pass index of 0.29, suggesting that it had rather transient dynamics.

The neuron's responses increased, reached a maximum, and then decreased for increasingly larger diameters of grating patches (Fig. 1*C*). We fit these responses with a ratio-of-Gaussians function (Cavanaugh et al. 2002a), from which we determined a $SIZE_{75}$ measure and an SI. $SIZE_{75}$ corresponded to the stimulus diameter at which the cell reached 75% of its maximal response. SI indicated the strength of surround suppression: an SI value of 0 corresponded to a cell that did not show any surround suppression; an SI value near 1 corresponded to a cell that was fully suppressed to baseline by large gratings. The example neuron had a $SIZE_{75}$ of 3.0° and an SI of 0.07, indicating a small amount of surround suppression.

Finally, the neuron's responses increased and then saturated at increasing stimulus contrasts (Fig. 1*E*). We fit the contrast responses with a hyperbolic ratio (Albrecht and Hamilton 1982; Naka and Rushton 1966) from which we estimated the c_{50} contrast and the slope, corresponding to the contrast needed to reach at least half of the fitted response at the highest contrast and the slope of the fitted response at c_{50} contrast, respectively. The example neuron had a c_{50} of 0.06 and a slope of 5.2.

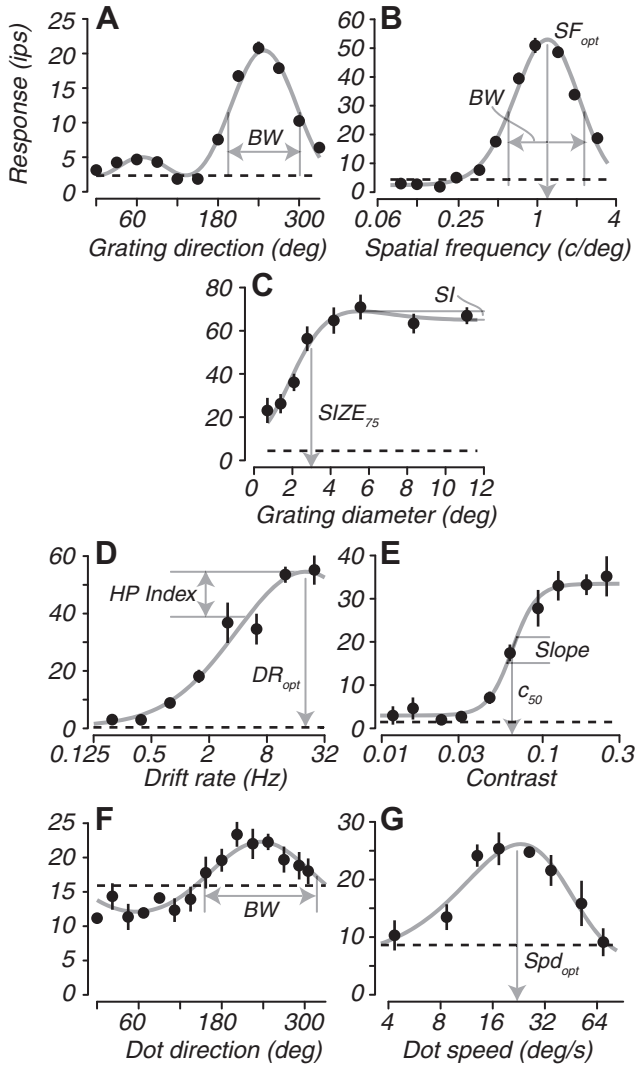

Fig. 1. Fitted tuning functions and derived response measures for a representative MT cell. Filled circles depict average firing rates (across trials) at tested stimulus values. Error bars indicate SE across trials. Dashed lines indicate baseline measures of firing rates. Gray curves represent best-fitting tuning functions describing the measured responses (see Table 1). *A–E* show responses for drifting sinusoidal gratings; *F* and *G* show responses for coherent random-dot textures. *A*: responses as a function of the direction of 50%-contrast gratings (ips, impulses/s). We derived a bandwidth measure (BW; full width at half-maximum height) from the best-fitting double von Mises function. *B*: responses as a function of the spatial frequency of drifting gratings. We derived the optimal spatial frequency (SF_{opt}; in cycles/deg, c/deg) and tuning bandwidth (BW; in octaves, full width at half-maximum height) from the best-fitting log-Gaussian. *C*: responses as a function of the diameter of a patch of otherwise optimal grating. We extracted a $SIZE_{75}$ measure and a suppression index (SI) from the best-fitting ratio-of-Gaussian function. $SIZE_{75}$ is defined as the smallest stimulus diameter that elicited 75% of the maximum response, and SI indicates the relative suppression from the maximum response at the largest stimulus diameter. *D*: responses as a function of the drift rate of a grating stimulus. The response was fit with a log-Gaussian, from which we extracted the optimal drift rate (DR_{opt}; in Hz) and a temporal high-pass index (HP index, or the slope of the response between DR_{opt} and ¼ of DR_{opt}). *E*: responses as a function of grating contrast. We extracted a c_{50} and a slope measure from the best-fitting hyperbolic ratio function. c_{50} is the contrast that elicited half of the fitted maximal response, and slope indicates the steepness of the fitted response at c_{50}. Baseline measures in *A–E* come from epochs in which a gray screen at the mean luminance was presented. *F*: responses as a function of the direction of random-dot textures. We fit the responses with the same double von Mises function as for grating directions in *A*, from which we derived the bandwidth measure (BW). *G*: responses as a function of the speed of random-dot textures moving in the preferred direction. The response was fit with a log-Gaussian, from which we derived the optimal speed (Spd_{opt}; in deg/s). Baseline measures in *F* and *G* come from epochs in which zero-coherence random motion was presented and are elevated because this cell responded to such motion (Britten et al. 1993).

Distributions of Tuning Properties in V1 and MT

Distributions of response measures derived from the fits across the entire population of MT neurons are shown in Fig. 2, *C–H* (black). Additionally, we also estimated a directionality index (DI; Fig. 2*A*) and an orientation selectivity index (OSI; Fig. 2*B*) from the data. Cells with DI values near or greater than 1 were highly direction-selective (a DI value >1 indicates a cell that had responses that were suppressed below baseline in the opposite direction); cells with DI values near 0 were nondirectional. OSI values ranged from 0 to 1, where 0 indicated equal responses to all orientations and 1 indicated responses only to gratings at a single orientation. We compared these distributions to similar or identical measures obtained from a control population of V1 cells (Fig. 2, *A–H*, orange).

In agreement with previous findings, most cells in MT were highly direction-selective, with a mean DI at 1.0, compared with a mean DI of 0.38 for V1 cells (Fig. 2*A*). OSI values for MT neurons (mean = 0.41) were more narrowly distributed than those for V1 cells, which tended to have more extreme values (Fig. 2*B*). This reflected the fact that, compared with V1 cells, MT neurons were more consistently orientation selective (a necessary condition for direction selectivity, Fig. 2*A*) but also tended to exhibit broader direction bandwidths (Fig. 2*C*). OSI is closely related to direction bandwidth; a larger bandwidth is associated with lower

orientation selectivity. Compared with V1 neurons, MT neurons also tended to show lower spatial frequency preferences (Fig. 2*D*), broader spatial frequency bandwidth (Fig. 2*E*), greater stimulus diameter preferences (Fig. 2*G*), and less surround suppression (Fig. 2*F*). These findings show that MT neurons have larger receptive fields and broader spatial tuning than V1 cells at equivalent eccentricities. Additionally, MT cells also tended to prefer higher drift rates than V1 cells (Fig. 2*H*). All the differences between V1 and MT populations were statistically significant ($P < 0.001$).

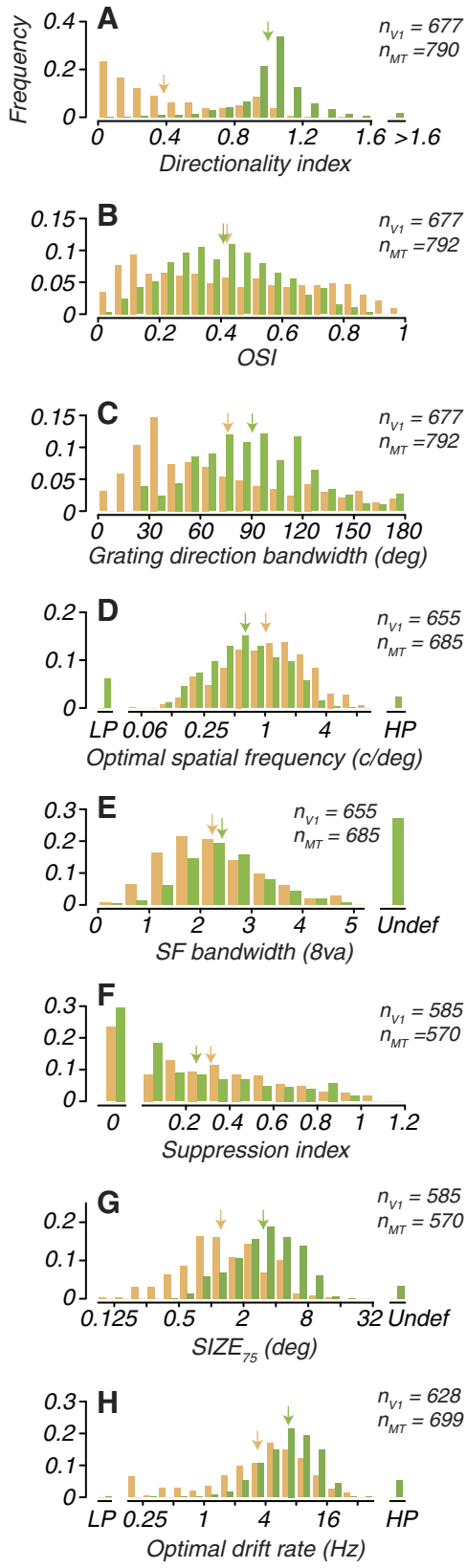

We used the baseline R_0 from the fit (*Eq. 2*) to derive the tuning bandwidths for grating direction and consequently might have underestimated the bandwidths for cells whose responses did not fall to the true baseline. As a check, we made an alternative measure of bandwidth by computing the width at half-height of the fitted response after adjusting for baseline using the measured spontaneous rate (rather than that estimated from the fit). This yielded a mean bandwidth of 86.4°, compared with the original estimate of 90.4° (Fig. 2*C*, black; $P = 0.01$), suggesting that the original bandwidths were actually slight overestimated due to the fact that responses in anti-preferred directions were suppressed slightly below spontaneous (see DI > 0 in Fig. 2*A*).

Eccentricity

We examined how all of our measured response properties varied as a function of eccentricity in both MT and V1. As expected, the preferred spatial frequency of neurons decreased with eccentricity in both V1 and MT (MT: $r = -0.18$; V1: $r = -0.46$; $P < 0.0002$ in both cases), but the decrease was more gradual in MT compared with that in V1 ($P < 0.001$, permutation test; Fig. 3*A*). V1 neurons preferred higher spatial frequencies than MT neurons at lower eccentricities, but the difference in preferred spatial frequencies between the two populations diminished at higher eccentricities. The criterion receptive field diameter (SIZE$_{75}$) increased with eccentricity (MT: $r = 0.19$; V1: $r = 0.40$; $P < 0.0002$ in both cases), but the increase was also more gradual in MT than in V1 ($P < 0.001$, permutation test; Fig. 3*B*).

Compared with V1, the receptive fields of MT neurons are more enlarged in space than changed in their preferred spatial frequency, meaning that on average there were more cycles of the optimal grating within their receptive fields ("cycles per RF", computed by multiplying the preferred spatial frequency of the cell by its receptive field size) than in V1 neurons (Fig. 3, *C* and *D*). The preferred number of cycles per RF increased

Fig. 2. Distributions of response measures in MT and V1. Green bars indicate response measures in MT neurons; orange bars denote the corresponding response measures in V1 neurons. *A*: directionality index (DI). DI values near 0 correspond to cells that are nondirectional; DI values near or greater than 1 correspond to cells that are highly direction-selective. *B*: orientation selectivity index (OSI). OSI is based on a vector measure of response to gratings of varying orientations, with values near 1 indicating greater orientation selectivity. *C*: direction tuning bandwidth to gratings. Bandwidth corresponds to the full width (in degrees) at half-maximal height of the fitted, baseline-subtracted response. *D*: optimal spatial frequency, derived from fits to suitable functions (Fig. 1*B*). Low-pass (LP) and high-pass (HP) cells had responses that were maximal at the lowest or highest spatial frequency presented, respectively. *E*: spatial frequency tuning bandwidth. Bandwidth corresponds to the full width (in octaves) at half-height of the fitted, baseline-subtracted response (Fig. 1*B*). The value "Undef" is given to cells whose responses did not drop by half on either side of the tuning curve. *F*: suppression index (SI; Fig. 1*C*). SI values near 0 indicate no suppression for large stimulus sizes. *G*: SIZE$_{75}$, stimulus diameter that evoked 75% of the maximal response. The value "Undef" is given to cells for which the fit did not define a diameter. *H*: optimal drift rate, calculated from fits as in *D* (Fig. 1*D*). n_{V1}, no. of V1 neurons; n_{MT}, no. of MT neurons.

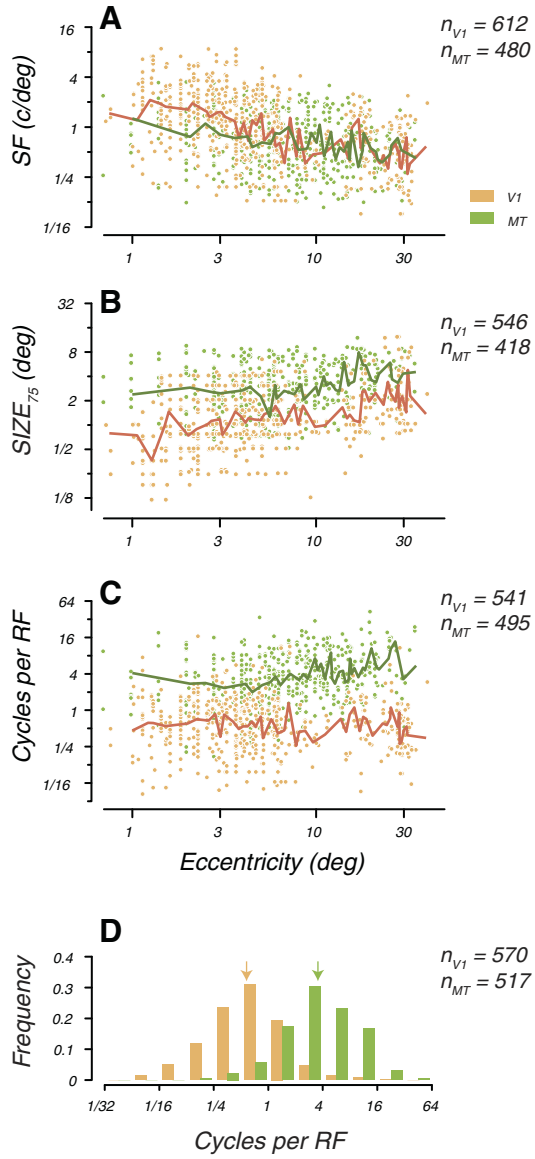

Fig. 3. Spatial properties and eccentricity. Green indicates MT neurons; orange indicates V1 neurons. *A*: scatter plot of optimal spatial frequency (SF) and receptive field eccentricity. *B*: scatter plot of receptive field diameter ($SIZE_{75}$) and receptive field eccentricity. *C*: scatter plot of the product of optimal spatial frequency and receptive field diameter (i.e., cycles of the optimal grating that fit within the receptive field, cycles per RF) and receptive field eccentricity. *D*: distributions of the number of cycles of the optimal grating per receptive field (as in *C*) summarized across all receptive field eccentricities.

slightly with eccentricity in MT neurons ($r = 0.29$; $P < 0.0002$) but not in V1 neurons ($r = -0.09$; $P = 0.02$). For this measurement in V1, the receptive field size corresponded to the stimulus diameter evoking 95% of the maximal response. For many MT cells, the receptive field mapped with small stimuli is larger than the size of the most effective stimulus patch (Raiguel et al. 1995). We therefore took the size estimate for MT receptive fields from hand maps of the fields rather than from area summation measurements.

Overall, we found that the dependence of spatial properties on eccentricity was less pronounced in MT than in V1. Additionally, the optimal number of cycles per RF depended substantially on eccentricity in MT neurons but less so in V1 neurons.

MT Population Characterized by the Pattern Index

We measured pattern direction selectivity in MT cells using 50%-contrast drifting sinusoidal gratings and with plaid patterns made by adding two such gratings oriented 120° apart (Fig. 4*A*). To quantify pattern motion selectivity, we computed the partial correlations between the cell's actual response to plaids and predictions based on standard models of pattern and component selectivity (Movshon et al. 1985). The predicted pattern-selective response to plaids was the same as the cell's measured grating response (Fig. 4*A*, red curve). The predicted component-selective response was the sum of two of such grating tuning curves, each shifted by an appropriate amount in angle to account for the direction of the plaid stimulus and baseline subtracted (Fig. 4*A*, blue curve). The correlations R_p and R_c were converted into Z scores (Z_p and Z_c, respectively) using Fisher's r-to-Z transformation to stabilize their variance (Smith et al. 2005). A value of 1.28 was used as the class boundary for Z_p and Z_c, equivalent to $P = 0.1$ (Fig. 4*B*). A cell was classified as PDS if Z_p exceeded Z_c by at least 1.28 or if $Z_p > 1.28$ when Z_c was negative. Conversely, a cell was classified as CDS if Z_c significantly exceeded Z_p. A cell that met neither criterion was unclassified. We term the difference, $Z_p - Z_c$, the "pattern index." Pattern index varied continuously across the population of MT neurons (Fig. 4*C*). The pattern index did not depend on eccentricity ($r = -0.01$, $P = 0.39$).

Direction Selectivity Measures and Pattern Index

We examined the selectivity profiles of the MT cells to grating and dot stimuli in relation to the pattern index. Cells that were more PDS tended to be more direction-selective, as indicated by the robust positive correlation between pattern index and DI ($r = 0.25$, $P < 0.0002$; Fig. 5*A*). Larger pattern selectivity was also strongly associated with a broader direction tuning bandwidth for grating stimuli ($r = 0.35$, $P < 0.0002$; Fig. 5*B*). In contrast, there was no correlation between pattern index and direction tuning bandwidth for dot textures ($r = -0.05$, $P = 0.242$; Fig. 5*C*). Bandwidth estimates determined by using the measured spontaneous rate as the baseline (see *Distributions of Tuning Properties in V1 and MT* above) yielded similar results.

Cells that were PDS tended to respond more robustly to complex motion stimuli (both plaids and dots) than to gratings. We compared the measured maximal firing rates for plaid and grating stimuli and found that PDS cells responded more strongly to a plaid (composed of two 50%-contrast gratings) than to a single 50%-contrast grating (average response ratio = 1.7, $P = 0.001$), whereas CDS cells showed more nearly equal responses to both (average response ratio = 1.2, $P = 0.004$; vs. response ratio for PDS: $P < 0.0001$; Fig. 5*D*). This highlights one of the hallmarks of pattern selectivity, in which CDS cells only respond to one of the component gratings in the plaid stimuli, whereas PDS cells integrate information from both gratings. In addition, CDS cells responded poorly to dots compared with gratings (average response ratio = 0.8, $P = 0.007$), whereas PDS cells tended to respond better to dots (average response ratio = 1.6, $P = 0.0003$; vs. response ratio for PDS: $P = 0.001$; Fig. 5*E*), consistent with the idea that PDS cells were able to integrate information from a broader spatiotemporal spectral range.

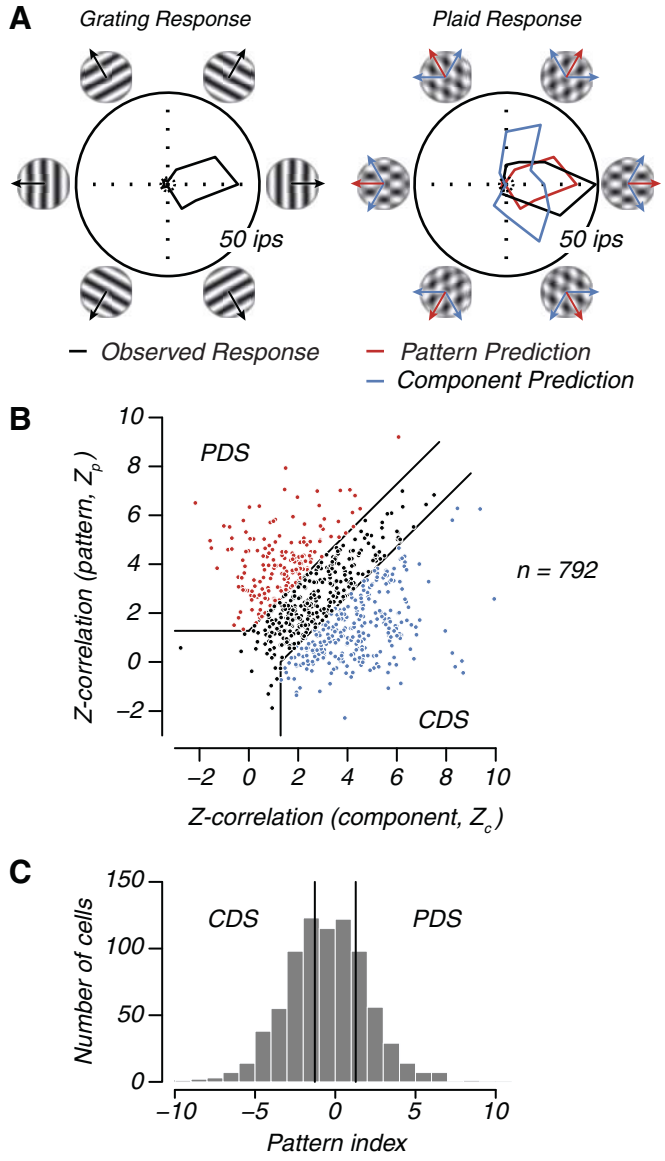

Fig. 4. Pattern and component direction selectivity. *A*: stimuli used to probe pattern direction selectivity and the corresponding responses of an example MT cell. Radial axis gives response magnitude of the cell, and the angular axis gives the direction of motion. *Left*, the cell showed a selective response to a grating drifting rightward (black curve). *Right*, plaid stimuli are made by summing 2 gratings 120° apart. The cell responded selectively to a plaid drifting to the right, conforming to the pattern prediction (red curve) rather than the component prediction (blue curve). Small black circles at the origin denote the spontaneous rate. *B*: pattern selectivity across the whole population. *Z*-transformed partial correlations between the measured plaid response of a cell and its component and pattern predictions (Z_c and Z_p, respectively) are plotted against each other. Pattern index is defined as $Z_p - Z_c$: cells with significant, large positive pattern indexes are classified as pattern-direction selective (PDS; red), and those with significant, large negative pattern indexes are classified as component-direction selective (CDS; blue). Unclassified cells are shown in black. Black lines indicate class boundaries, corresponding to values of pattern index at −1.28 and +1.28, or a statistical classification threshold of $P = 0.1$; $n_{total} = 792$, $n_{PDS} = 179$, $n_{CDS} = 296$. *C*: distribution of pattern index. Dashed lines indicate class boundaries for PDS and CDS cells.

Spatial Response Properties and Pattern Index

We determined spatial selectivities of the cells from their spatial frequency and stimulus diameter tuning functions. Pattern index showed a weak but significant negative correlation with the log of the optimal spatial frequency of the cell ($r = -0.07$, $P = 0.032$; Fig. 6*A*), indicating that cells that were more pattern-selective tended to prefer lower spatial frequencies. This effect was statistically significant only for the 348 cells tested with the continuous stream stimulation protocol, but not for the 279 tested using discrete-trial presentations (Table 2). We found no correlation between pattern index and spatial frequency bandwidth ($r = 0.00$, $P = 0.488$; Fig. 6*B*).

For cells whose responses did not fall when spatial frequency was at the limits of testing, we could define no preferred spatial frequency. Of these, 42/685 cells showed a low-pass tuning (i.e., their response did not fall at the lowest spatial frequency tested; Fig. 2*D*, LP). We examined these cells separately to see whether their pattern index differed from that of the overall population. The mean pattern index across the low-pass cells was −1.23, compared with −0.54 across the overall population ($P = 0.0484$, permutation test), indicating that cells with low-pass responses were predominantly component selective. This was consistent with the overall trend that spatial frequency preference was negatively correlated with the pattern selectivity (Fig. 6*A*). For a few cells (16/690), the highest spatial frequency tested evoked the maximal response (Fig. 2*D*, HP); these cells were not considered as a separate population.

The $SIZE_{75}$ measure, obtained from the ratio-of-Gaussians fitted responses to grating patches of varying diameters, corresponds to the smallest diameter of a grating patch that evoked at least 75% of the fitted maximal response (Fig. 1*C*). Pattern index was negatively correlated with log $SIZE_{75}$ ($r = -0.11$, $P = 0.007$), indicating that cells with higher pattern indexes tended to prefer small stimulus diameters (Fig. 7*A*). $SIZE_{75}$ was undefined for a small number of cells for which the response amplitude was accelerating even at the largest presented stimulus diameter (19/570 cells; Fig. 2*G*, Undef). When examined separately, these cells did not have pattern indexes that were significantly different from that of the overall population ($P = 0.387$; permutation test).

We quantified the strength of a cell's surround suppression using a suppression index (SI; Cavanaugh et al. 2002a). Many cells (169/570) had SI equal to 0; i.e., they did not show any attenuation in response amplitude at the largest stimulus diameter presented. These zero-valued suppression indexes did not occur only in cells with large diameter preferences, but rather occurred in cells preferring the entire range of stimulus diameters (data not shown).

We examined the distribution of SI separately for each pattern-selective population (Fig. 7*C*). Cells that were more pattern selective tended to include a smaller proportion of cells with SI equal to 0 (bottommost bin of each histogram), indicating that they were more likely to show surround suppression. Of PDS cells ($n_{PDS} = 144$), only 19% had SI = 0, compared with 35% of CDS cells ($n_{CDS} = 206$) and 31% of unclassified cells ($n_{Unc} = 220$). This difference in the proportions of zero-valued SI was highly significant between populations (PDS vs. CDS, $P < 0.0002$). For values of SI greater than 0, there was also a statistically significant correlation between pattern index and SI ($r = 0.10$, $P = 0.020$; Fig. 7*B*). Cells that were more pattern selective also tended to show greater surround suppression.

Overall, cells that were more pattern selective tended to prefer lower spatial frequencies, but the relationship between

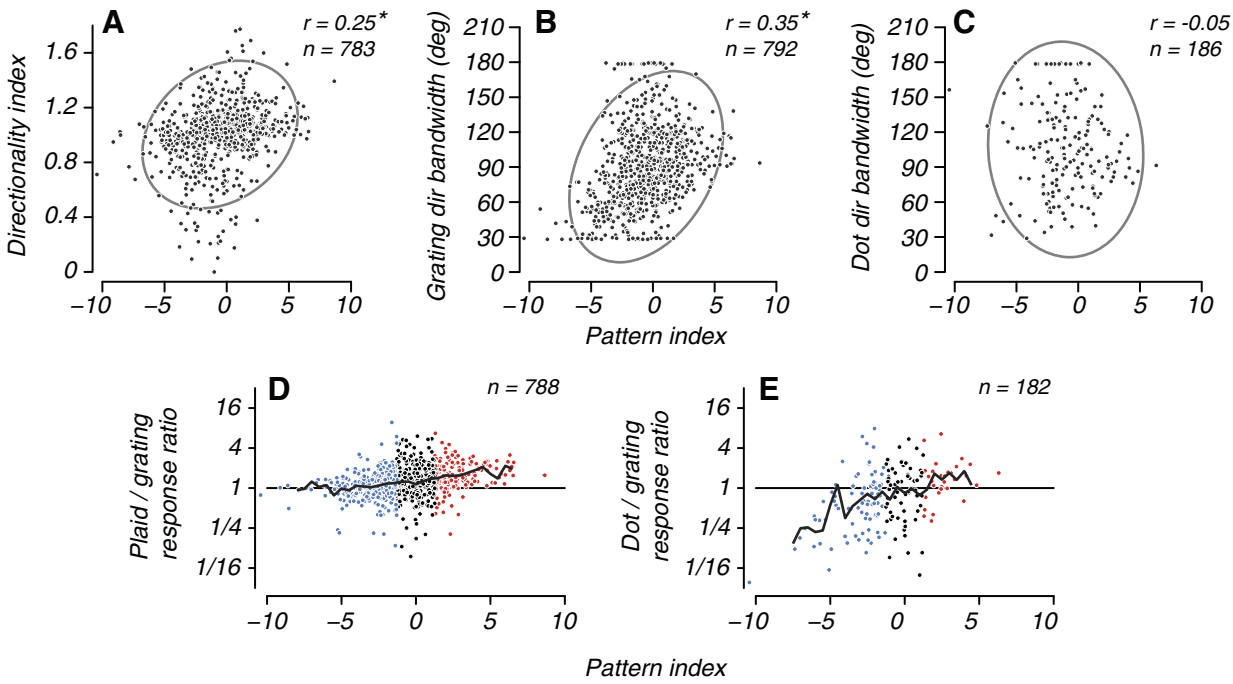

Fig. 5. Direction selectivity and pattern index. Each filled circle indicates an individual MT cell. In *A–C*, the light blue curve shows the 95% covariance ellipse; the tilt of the ellipse corresponds to the strength of the correlation between the 2 measures under study. *A*: pattern index is robustly correlated with direction selectivity for gratings, as quantified by DI ($r = 0.25$, $P < 0.0002$ by permutation test). *B*: scatter plot of pattern index against grating-direction tuning bandwidth (see Fig. 1*A*). Pattern index is positively correlated with grating direction bandwidth ($r = 0.35$, $P < 0.0002$). *C*: scatter plot of pattern index against dot-direction tuning bandwidth (see Fig. 1*F*). Pattern index shows a negative but statistically insignificant correlation with dot direction bandwidth ($r = -0.05$, $P = 0.242$). *D*: scatter plot of pattern index against the ratio of the measured maximal plaid response to maximal grating response. Thick black curve shows the running mean of response ratio. Gratings were shown at 50% contrast, and plaids were composed of 2 such gratings 120° apart. *E*: scatter plot of pattern index against the ratio between maximal responses for high contrast random dot textures and those for gratings (same format as *D*).

preferred spatial frequency and pattern selectivity was weak. We found no correlation between spatial frequency bandwidth and pattern selectivity. Cells that were more pattern selective also preferred smaller stimulus sizes, perhaps related to their stronger surround suppression. In combination, these factors mean that pattern-selective cells on average preferred slightly fewer cycles of the optimal grating in their receptive fields (the geometric mean of cycles per RF was 3.4 for CDS and 4.1 for PDS cells, $P = 0.04$).

Temporal Response Properties and Pattern Index

We next examined how pattern direction selectivity related to the temporal response properties of the cell. Pattern index was positively correlated with the log of the optimal drift rate ($r = 0.19$, $P < 0.0002$; Fig. 8*A*), indicating that cells that were more pattern selective tended to prefer higher drift rates. To assess the shape of the tuning response for drift frequencies, we determined a temporal high-pass index, the slope of the low-frequency (high pass) limb of the tuning function (Fig. 1*D*). High-pass indexes near 0 indicated cells with low-pass temporal frequency tuning, whereas high-pass indexes near 1 indicated tuning that was high- or band-pass. Pattern index was correlated with the high-pass index ($r = 0.11$, $P = 0.002$; Fig. 8*B*), indicating that pattern-selective cells tended to show more high- or band-pass temporal tuning than low-pass behavior.

We could not measure the optimal drift rate for a fraction of the cells that did not saturate in response amplitude even at the extremes of the drift rates presented. A few cells (2/699) showed a low-pass response (Fig. 2*H*, LP), but were too rare to yield any meaningful analyses. Lack of attenuation at high drift rates (37/699 cells, Fig. 2*H*, HP) reflected experimental display limits; these cells were therefore not considered as a separate population and did not show pattern indexes that differed from that of the overall population ($P = 0.325$).

Speed tuning functions obtained using dot textures were available for a small number of cells. Cells with higher pattern indexes tended to have higher speed preferences ($r = 0.20$, $P = 0.033$; Fig. 8*C*). The mean pattern index across cells with low-pass speed tuning responses (5/86 cells) was −1.57 (compared with −0.54 across the overall population), indicating that these cells were predominantly component selective. Speed preference is closely related to the optimal spatial frequency and temporal drift rates of the cell; the optimal speed for a drifting grating is given by the preferred temporal frequency divided by the preferred spatial frequency (Priebe et al. 2006). We therefore estimated the optimal grating speed from each cell's preferred spatial and temporal frequencies and compared it with the optimal dot speed. As expected, these two measures corresponded well ($r = 0.79$, $P < 0.0002$, $n = 68$; Fig. 8*D*). Notably, most data lie below the diagonal, indicating that many cells preferred a higher dot speed than grating speed. Also as expected, the preferred speed for dots was highly negatively correlated with the preferred grating spatial frequency ($r = -0.70$, $P < 0.0002$, $n = 74$) and highly positively correlated with the preferred grating drift rate ($r = 0.50$, $P < 0.0002$, $n = 71$), suggesting that both spatial and temporal factors contribute to speed preference.

A number of temporal response properties correlated with pattern selectivity. Cells that were more pattern selective tended to prefer higher drift rates and higher speeds and were less likely to show low-pass tuning for drift rate.

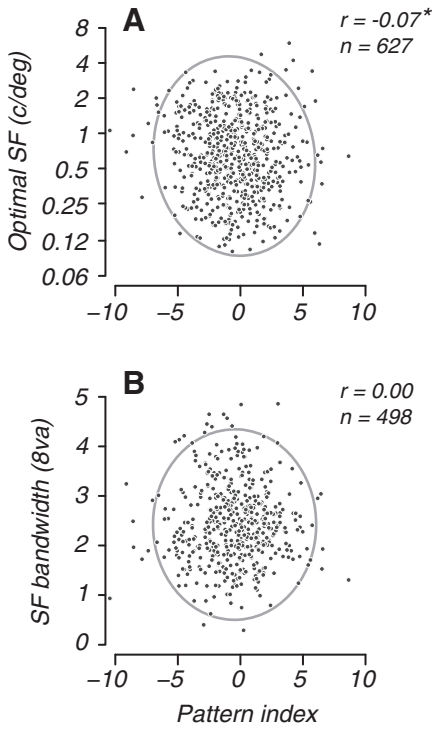

Fig. 6. Spatial frequency tuning and pattern index. In *A* and *B*, the light gray curve indicates the 95% covariance ellipse. *A*: scatter plot of pattern index against optimal spatial frequency (see Fig. 1*B*). Pattern index shows a negative correlation with spatial frequency preferences ($r = -0.07$, $P = 0.032$). Correlation (r) was computed with the log of spatial frequency; cells with responses that did not attenuate at the highest or lowest presented stimulus value were excluded from the correlation analysis. *B*: scatter plot of pattern index against spatial frequency tuning bandwidth shows no correlation ($r = 0.00$, $P = 0.488$).

Contrast Response Properties and Pattern Index

Pattern index showed little relationship with contrast sensitivity (Fig. 9). The correlation was near zero with either log c_{50} (contrast needed to reach 50% of the maximal response; $r = -0.01$, $P = 0.445$; Fig. 9*A*) or with the log of the slope of the contrast response function at c_{50} ($r = -0.01$, $P = 0.442$; Fig. 9*B*). Using a fitted semi-saturation parameter β (*Eq. 7*) rather than the derived c_{50} produced similar results. Curiously, the correlation of pattern index with log c_{50} was positive and significant for the 148 cells tested with discrete-trial presentations ($r = 0.22$, $P = 0.003$) and negative and significant for the 220 cells tested with continuous stream presentations ($r = -0.14$, $P = 0.02$). This may reflect a subtle difference in susceptibility to contrast adaptation between pattern and component cells, since the discrete-trial protocol has a less profound adapting effect than the continuous stream (Smith et al. 2005).

Interaction of Spatial and Temporal Representations in PDS and CDS Populations

We also investigated the relationship between spatial and temporal preferences across the MT population and whether the relationship was related to pattern selectivity. Preferred spatial frequency and drift rate were negatively correlated for PDS cells ($r = -0.33$, $P < 0.0002$) but were not correlated for CDS cells ($r = -0.02$, $P = 0.43$; Fig. 10). Note that this relationship is not to be confused with the separability of spatial and temporal tuning in an individual cell. Rather, it shows how MT cells with different spatial and temporal frequency preferences sample spatiotemporal frequency space. Cells that were more pattern selective tended to overrepresent spatiotemporal frequencies along a diagonal, preferring stimuli either with low spatial frequency and high temporal frequency, or vice versa. This relationship was not present in CDS cells, whose representations of spatial and temporal frequencies were mutually independent. This interdependence of spatiotemporal preferences in PDS cells is reminiscent of the properties of spatial and temporal frequency channels estimated psychophysically from contrast detection measurements (Kelly 1979; Robson 1966).

We wondered whether this relationship was confounded by receptive field eccentricity, which can affect frequency preferences (Fig. 3). Eccentricity data were available for 94 PDS cells and 189 CDS cells with spatial frequency and drift rate measurements. We divided the data into two roughly equal groups, with eccentricities greater or less than 7°. For each group, we computed the correlation between spatial frequency and drift rate and assessed the confidence intervals of the correlation values with bootstrapping. The correlations for the low- and high-eccentricity PDS cells were both near −0.3 and significantly different from 0. The correlations for the low- and

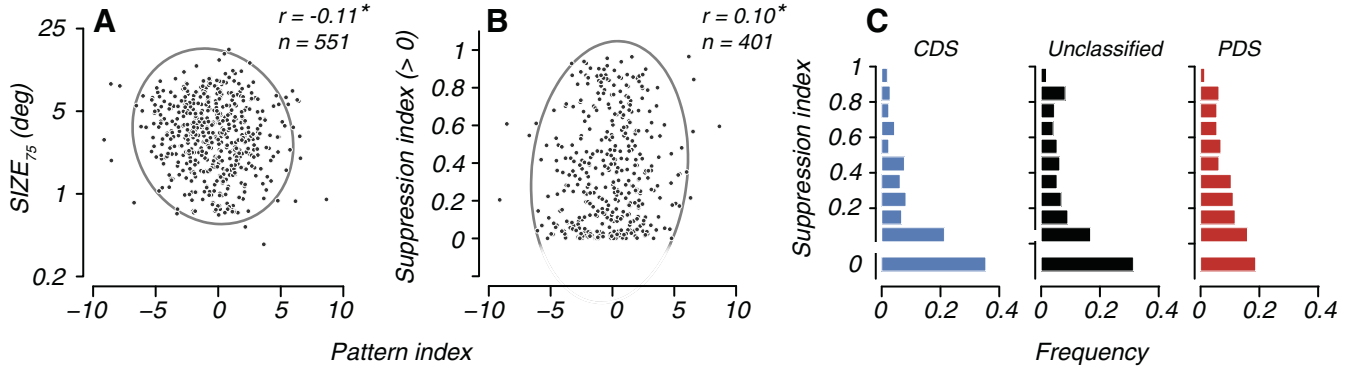

Fig. 7. Size tuning and pattern index. In *A* and *B*, the light blue curve indicates the 95% covariance ellipse. *A*: scatter plot of pattern index against $SIZE_{75}$ (see Fig. 1*C*) of the cell. Pattern direction selectivity is negatively correlated with the optimal diameter of the grating patch ($r = -0.11$, $P = 0.007$). Correlation was computed with the log of $SIZE_{75}$. *B*: scatter plot of pattern index against SI for those cells with SI > 0. Pattern index is positively correlated with the non-zero SI values ($r = 0.10$, $P = 0.020$), indicating that pattern selectivity is correlated with stronger suppression. *C*: distribution of SI in CDS, unclassified, and PDS cell populations. The bottommost bin of each distribution contains cells with SI = 0 (no suppression). Each distribution was normalized by the number of cells in the respective population (206 CDS, 220 unclassified, and 144 PDS).

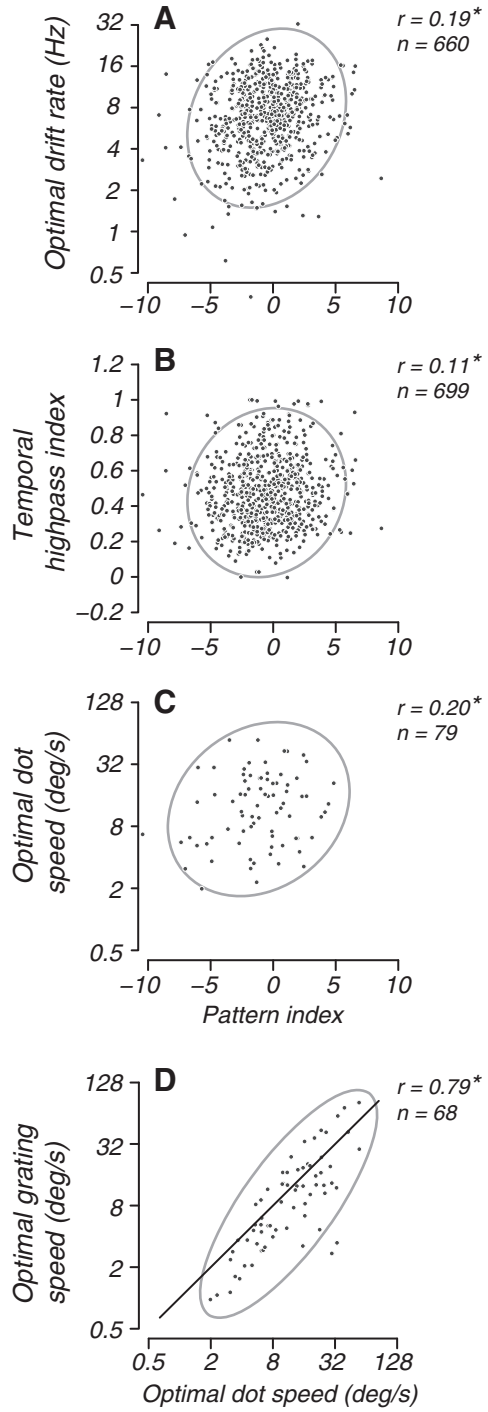

Fig. 8. Temporal properties and pattern index. In *A–D*, the light gray curve indicates the 95% covariance ellipse. *A*: scatter plot of pattern index against the optimal drift rate for gratings (see Fig. 1*D*). Pattern selectivity shows a highly significant positive correlation with drift rate ($r = 0.19$, $P < 0.0002$). Correlation (r) was computed with the log of drift rate; cells with responses that did not attenuate at the highest or lowest presented stimulus value were excluded from the correlation analysis. *B*: scatter plot of pattern index against temporal high-pass index for drift rate tuning (see Fig. 1*D*). Pattern index shows a positive correlation with band-pass index ($r = 0.11$, $P = 0.002$). *C*: scatter plot of pattern index against the optimal speed of dot textures (see Fig. 1*G*). Correlation (r) was computed with the log speed. Pattern index is positively correlated with speed ($r = 0.20$, $P = 0.033$). *D*: scatter plot of optimal dot speed against optimal grating speed (taken as the ratio of the preferred temporal to spatial frequencies for each cell). The 2 speed measures are positively correlated ($r = 0.79$, $P < 0.0002$).

high-eccentricity CDS cells were not significantly different from 0. Within the limits imposed by the available sample sizes, we conclude that eccentricity did not introduce a confound into this analysis.

Response Dynamics for Pattern- and Component-Selective Cells

We examined whether the response dynamics differed between pattern- and component-selective populations; only cells with responses measured using the rapid, continuous stream stimulus presentation protocol were included, because they contained enough trials to allow for a precise estimate of latency using the method of Smith et al. (2005; see MATERIALS AND METHODS). We used this latency estimate to align spike times to the onset of the response. The plaid and grating histograms of each cell were normalized by the highest spike count from either the plaid or the grating response, and the resulting normalized, time-aligned histograms were averaged to provide an estimate of population response dynamics.

PDS cells responded more strongly to plaids than to gratings throughout the entire response epoch (Fig. 11, light and dark red), whereas CDS cells responded roughly equally to both types of stimuli (Fig. 11, light and dark blue). Compared with CDS cells, PDS cells showed enhanced responses to plaids (light red vs. light blue) and suppressed responses to gratings (dark red vs. dark blue). These results are consistent with those showing the average response ratio based on total spike counts (Fig. 5*D*), while revealing how response differences evolved over time. Responses started earlier and rose more sharply for

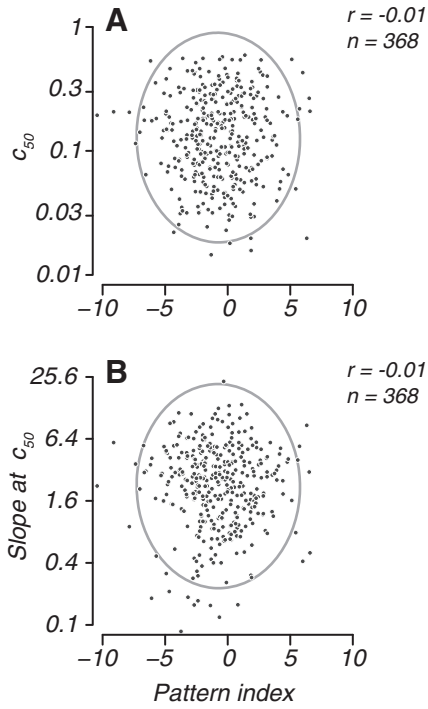

Fig. 9. Contrast response and pattern index. In *A* and *B*, the light gray curve indicates the 95% covariance ellipse. *A*: scatter plot of pattern index against c_{50} (see Fig. 1*E*). Correlation (r) was computed with the log c_{50}; no correlation was found between pattern index and c_{50} ($r = -0.01$, $P = 0.445$). *B*: scatter plot of pattern index against slope of the contrast response function at c_{50} (see Fig. 1*E*). Correlation (r) was computed with the log slope; no correlation was found between pattern index and slope ($r = -0.01$, $P = 0.442$).

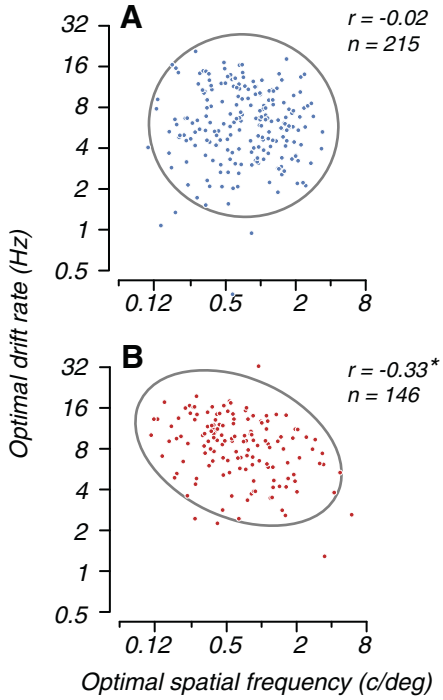

Fig. 10. Scatter plot of optimal spatial frequency against optimal drift rate. In *A* and *B*, the light blue curve indicates the 95% covariance ellipse. *A*: CDS cells. Preferences of spatial frequency and drift rate show no correlation with each other ($r = -0.02$, $P = 0.43$). *B*: PDS cells. Preferences of spatial frequency and drift rate are negatively correlated ($r = -0.33$, $P < 0.0002$).

grating stimuli than for plaids in both PDS and CDS populations (Fig. 11, *right*), consistent with earlier observations (Smith et al. 2005). Note that our procedure of aligning the spike trains to response onset removed the influence of the latency differences between PDS and CDS cells reported earlier (Smith et al. 2005).

We found little difference in response dynamics between PDS and CDS populations. To quantify response transience, we computed a transience index, computed as early response/(early response + late response) (Maunsell and Gibson 1992). We defined early response to be the number of spikes within the first 50 ms after response onset, and late response to be those in the 50-ms period starting 200 ms after response onset. Both response measures were baseline subtracted. A cell with a strong early response and no significant late response would have a transience index near 1; a cell showing equal early and late responses would have an index near 0.5. We found no significant correlation between the pattern index and response transience for responses to gratings ($r = -0.02$, $P = 0.337$) or plaids ($r = -0.003$, $P = 0.477$). One might expect response transience to be related to the temporal high-pass index, which also quantifies the cell's inferred step response in the time domain from temporal frequency tuning measurements. However, surprisingly, we found no significant correlation between response transience and the temporal high-pass index to gratings ($r = 0.01$, $P = 0.40$). Response dynamics might not match frequency measurements for a variety of reasons, including adaptation effects on the time course of the step response (Lisberger and Movshon 1999; Tolhurst et al. 1980).

Because response dynamics can depend on the drift rate of the stimulus (Maddess et al. 1988), we performed the analyses again, after excluding cells with preferred drift rates that differed by more than an octave from the drift rate at which plaid and grating stimuli were presented, and obtained qualitatively similar results.

Multivariate Analysis and Dimensionality Reduction

Our results reveal correlations between pattern index and a large number of spatial and temporal variables, but some of those variables also covary with each other. We therefore performed a multiple regression analysis by regressing pattern index against 10 *Z*-scored predictor variables (Fig. 12*A*). This provides a complementary method to assess the strength of covariability between each of these variables and pattern index while controlling for covariability among the predictor variables. A drawback is that this only allowed us to analyze the small subset of cells for which all measures were available, reducing the statistical power to reveal weak relationships. Confirming our earlier findings, grating direction bandwidth and optimal drift frequencies predicted pattern index reliably, as indicated by their positive regression coefficients, but the other variables used in the regression did not yield coefficients that were individually significantly different from 0, except for eccentricity, which we included because it covaried with other properties of interest (e.g., spatial frequency; Fig. 3*A*) and therefore explained some of their variance (Fig. 12*A*).

We further explored underlying relationships among the response parameters by performing a PCA on the same 10 measurements. We reasoned that if the relationships among the various spatial and temporal response properties were captured by a small number of hidden dimensions, then PCA would yield a small number of principal components (PCs) that captured most of the variance in the data. Instead, we found that the relative variance explained by each PC decreased gradually and that each PC only explained a relatively small amount of the variance in the overall data (Fig. 12*B*). This suggests that the high-dimensional data cannot be reduced to a succinct representation with a small number of dimensions. Additionally, variances explained by the first few PCs were similar, indicating that the ranking of these PCs was rather fragile and might be easily perturbed by noise.

We also wondered whether transformation into PC space yielded any dimensions that were more predictive of pattern selectivity than the original measures. We therefore performed a multiple regression by regressing pattern index against the PC scores (i.e., representation of the data in PC space). If

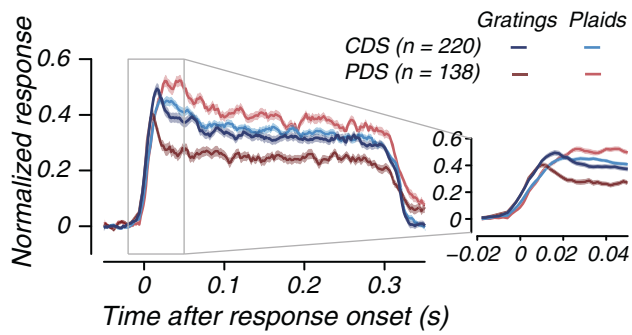

Fig. 11. Average normalized and baseline-subtracted peristimulus time histograms (PSTHs) of PDS and CDS cells to plaid and grating stimuli, aligned to response onset. Dark and pale red curves indicate PDS response to gratings and plaids, respectively; dark and light blue curves indicate CDS response to gratings and plaids, respectively. Error bars indicate SE across cells.

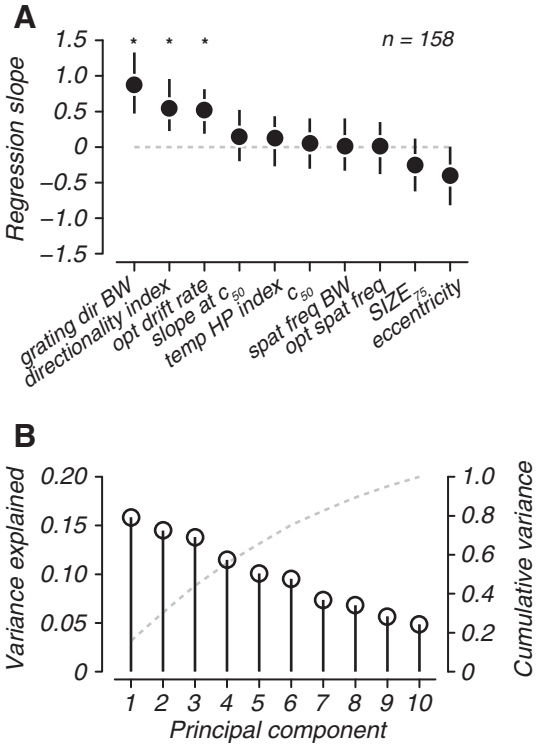

Fig. 12. Multivariate analysis and dimensionality reduction. *A*: multiple regression of pattern index against 10 *Z*-scored response variables. Regression coefficients corresponding to the variables are plotted in order of magnitude and sign. Dotted line at regression slope of 0 indicates the variable does not predict pattern index. Error bars are 95% bootstrapped confidence intervals. Only grating direction bandwidth, directionality index, and optimal drift rate significantly predict pattern index (asterisks). *B*: principal component analysis on the 10 variables in *A*. Open circles represent variance explained by each principle component (PC), sorted by magnitude. Dotted line indicates the cumulative variance accounted for with the addition of each PC dimension. Cumulative variance rises gradually, indicating that no small number of PCs can account for the majority of variance in the data.

transformation into PC space accentuated the relationship with pattern selectivity, we would then expect the regression coefficients for at least one dimension of the PC scores to be higher than the highest found in the original data. This was not the case: the coefficients for the first three PC scores were no larger than those for the largest for the original data variables (data not shown), suggesting that no "natural axes" capturing the data (as given by PCA) predicted pattern selectivity better than the original variables.

DISCUSSION

We have presented the results of an analysis of a large set of physiological measurements of the responses of well-isolated single cells recorded from the visual cortex of anesthetized macaques in our laboratory in the course of other experiments. In those experiments, as part of the basic characterization of the cells we studied, we explored a standard set of stimulus-response relationships, and this report is an analysis of the structure of some of those relationships.

We first compared the responses of populations of cells recorded in the primary visual cortex, V1 (Cavanaugh et al. 2002a, 2002b; Hubel and Wiesel 1968), and in MT, an area known to have a high concentration of cells that show selective responses to the direction of motion (Maunsell and Van Essen 1983; Zeki 1974). In character with their presumed role in temporal and motion processing, cells in MT tended to respond well to stimuli with lower spatial frequencies and higher drift rates than cells in V1. MT cells tended to be less selective for orientation but more selective for direction of motion than V1 cells, and generally to be less selective for other spatiotemporal parameters than V1 cells.

Although comparison between V1 and MT was instructive, our main interest was the organization of cells in MT that show different motion selectivities to visual patterns. Some cells in MT, similarly to direction-selective cells in V1, respond to complex moving patterns as if they are sensitive only to individual, oriented components of those patterns: these cells are CDS. Other cells, which are not encountered in significant numbers in V1 but are found in MT and other downstream cortical areas, integrate information across stimulus components to give responses that depend on the motion of the whole pattern: these cells are PDS (Khawaja et al. 2009; Movshon et al. 1985; Nishimoto and Gallant 2011; Rodman and Albright 1989; Rust et al., 2006; Simoncelli and Heeger 1998; Smith et al. 2005; Stoner and Albright 1992). The basis of pattern selectivity has been intensely studied; it seems to emerge from a set of computations that depend both on the properties of particular afferents from earlier areas and also on different patterns of neural computation within area MT itself (Rust et al. 2006). The distinction between pattern and component cells is continuous rather than categorical, so the variations between cell types are smooth. To illuminate this variation, we used the data from our population of MT neurons to compare the properties of CDS and PDS cells with respect to a large family of stimulus-response relationships.

Some patterns emerged from this analysis that were expected and predicted from previous work. For example, previous work comparing plaid and grating responses (see Born and Bradley 2005) led us to expect the observation that pattern cells tend to be more strongly direction-selective than component cells (Fig. 5*A*) and tend to be relatively more selective (narrower tuning width) for the direction of complex stimuli (plaids, textures) than for the direction of simpler stimuli like gratings (Fig. 5, *B* and *C*). Pattern cells also showed enhanced responses to compound stimuli and attenuated responses to single gratings (Fig. 5, *D* and *E*), consistent with their broader recruitment of inputs from cells with a variety of direction preferences (Rust et al. 2006; Simoncelli and Heeger 1998; Smith et al. 2005).

A more subtle variation is also predicted by prior work. Rust et al. (2006) postulated that, to account for pattern motion selectivity, pattern cells in MT should receive strong input from cells in V1 with a strong "tuned" component of contrast gain control (equivalent to surround suppression as described by Sceniak et al. 1999; Cavanaugh et al. 2002a). This result is consistent with our finding that pattern cells showed stronger surround suppression than component cells (Fig. 7*C*), which in turn may account for the smaller receptive fields of pattern cells (Fig. 7*A*). These differences between pattern and component cells may reflect variations in the distribution of properties of their afferents (Livingstone et al. 2001; Nishimoto and Gallant 2011; Rust et al. 2006).

We expected to find differences in the spatial properties and selectivity of pattern and component cells on the basis of previous observations and models but were surprised to find

also that pattern cells tended to prefer higher temporal frequencies than component cells. Pattern cells preferred higher drift rates and were more band pass (rather than low pass) in their temporal frequency tuning (Fig. 8, *A* and *B*). However, pattern cells did not show more transient response dynamics than component cells (Fig. 11). Response dynamics might not match temporal frequency preferences for a variety of reasons; for example, it might be due to the effect of adaptation, which is not evident in the temporal frequency characterization (Lisberger and Movshon 1999). These differences in temporal frequency preferences between pattern and component cells do not readily map onto current models of the pattern motion computation, but they do tend to argue against serial models in which pattern cells are thought to emerge from neural circuits with inputs from MT component cells (Grzywacz and Yuille 1990; Movshon et al. 1985; Perrone and Krauzlis 2008): such models could not easily explain why pattern cells respond more vigorously to rapidly varying stimuli than do their inputs. Perhaps pattern cells receive inputs from cells in earlier areas or pathways that have relatively rapid temporal dynamics so that their responses at least partly reflect the properties of those inputs.

One peculiar finding is that the distribution of preferred spatial and temporal frequencies for pattern cells shows a strong negative correlation, whereas the same distribution for component cells shows no similar relationship (Fig. 10). The basis for this difference in the distribution of spatiotemporal preferences is unclear, but it is perhaps noteworthy that the distribution for pattern cells resembles in shape the human spatiotemporal contrast sensitivity surface (Kelly 1979; Robson 1966).

One simple outcome of our analysis would be to predict the degree of pattern selectivity from other cell properties. It is plain from the analyses we have presented (Figs. 5–10) that there is no strong simple correlation between pattern selectivity and any single property. This impression is reinforced by Fig. 12*A*, which plots the outcome of a regression analysis combining all the variables that we separately analyzed. We *Z*-scored the values of pattern index and 10 other measures and normalized them to have unit variance, and then computed a multiple linear regression of those on pattern index. Only three (direction bandwidth, direction selectivity, and optimal drift rate) were significantly related to pattern index. We then wondered whether a small number of multicomponent latent variables might explain the diversity of properties we observed. We performed a PCA and asked whether the most important components revealed by the analysis might have more concentrated explanatory power than the individual tuning measurements. The outcome is shown in Fig. 12*B*, showing the eigenvalues of the 10 principal components and the cumulative fraction of explained variance. This analysis reveals no small set of hidden variables that might account for the diversity of pattern selectivity in our data. Instead, the variance explained by the sequence of principal components fell smoothly and without inflection, suggesting that the main components of variation are independent and uncorrelated.

How are we to interpret the lack of singular organization in Fig. 12? Pattern selectivity is not explained by any single other receptive field feature or simple combination of features: we think that this is not accidental. The response preferences of the population of MT cells are arranged so that stimulus preferences are dispersed among all the dimensions represented by our measurements, including pattern selectivity. This dispersion in high dimensions gives the population of MT cells the ability to represent true motion for objects and scene elements with a diversity of associated spatial and temporal properties, just as one would want and expect for a system whose goal is to keep the animal informed about the nature and disposition of all of the many moving elements of the visual world.

ACKNOWLEDGMENTS

We thank members of the Movshon laboratory, past and present, for sharing data with us, for many kinds of help, and for many stimulating conversations.

GRANTS

This work was supported by NIH Grants EY002017 and EY004440 (to J. A. Movshon).

ENDNOTE

At the request of the authors, readers are herein alerted to the fact that additional materials related to this manuscript, consisting of a database containing the neuronal data analyzed here and Matlab code for extracting that data, may be found at the institutional website archive of one of the authors, which at the time of publication they indicate is http://hdl.handle.net/2451/34281. These materials are not a part of this manuscript and have not undergone peer review by the American Physiological Society (APS). APS and the journal editors take no responsibility for these materials, for the website address, or for any links to or from it.

DISCLOSURES

No conflicts of interest, financial or otherwise, are declared by the authors.

AUTHOR CONTRIBUTIONS

H.X.W. and J.A.M. conception and design of research; H.X.W. and J.A.M. analyzed data; H.X.W. and J.A.M. interpreted results of experiments; H.X.W. and J.A.M. prepared figures; H.X.W. and J.A.M. drafted manuscript; H.X.W. and J.A.M. edited and revised manuscript; H.X.W. and J.A.M. approved final version of manuscript; J.A.M. performed experiments.

REFERENCES

Albrecht DG, Hamilton DB. Striate cortex of monkey and cat: contrast response function. *J Neurophysiol* 48: 217–237, 1982.

Born RT, Bradley DC. Structure and function of visual area MT. *Annu Rev Neurosci* 28: 157–189, 2005.

Britten KH, Shadlen MN, Newsome WT, Movshon JA. Responses of neurons in macaque MT to stochastic motion signals. *Vis Neurosci* 10: 1157–1169, 1993.

Cavanaugh JR, Bair W, Movshon JA. Nature and interaction of signals from the receptive field center and surround in macaque V1 neurons. *J Neurophysiol* 88: 2530–2546, 2002a.

Cavanaugh JR, Bair W, Movshon JA. Selectivity and spatial distribution of signals from the receptive field surround in macaque V1 neurons. *J Neurophysiol* 88: 2547–2556, 2002b.

Dubner R, Zeki SM. Response properties and receptive fields of cells in an anatomically defined region of the superior temporal sulcus in the monkey. *Brain Res* 35: 528–532, 1971.

Grzywacz NM, Yuille AL. A model for the estimate of local image velocity by cells in the visual cortex. *Proc R Soc Lond B Biol Sci* 239: 129–161, 1990.

Hubel DH, Wiesel TN. Receptive fields and functional architecture of monkey striate cortex. *J Physiol* 195: 215–243, 1968.

Kelly DH. Motion and vision. II. Stabilized spatio-temporal threshold surface. *J Opt Soc Am* 69: 1340–1349, 1979.

Khawaja FA, Tsui JM, Pack CC. Pattern motion selectivity of spiking outputs and local field potentials in macaque visual cortex. *J Neurosci* 29: 13702–13709, 2009.

Levitt JB, Schumer RA, Sherman SM, Spear PD, Movshon JA. Visual response properties of neurons in the LGN of normally reared and visually deprived macaque monkeys. *J Neurophysiol* 85: 2111–2129, 2001.

Lisberger SG, Movshon JA. Visual motion analysis for pursuit eye movements in area MT of macaque monkeys. *J Neurosci* 19: 2224–2246, 1999.

Livingstone MS, Pack CC, Born RT. Two-dimensional substructure of MT receptive fields. *Neuron* 30: 781–793, 2001.

Maddess T, McCourt ME, Blakeslee B, Cunningham RB. Factors governing the adaptation of cells in area-17 of the cat visual cortex. *Biol Cybern* 59: 229–236, 1988.

Maunsell JH, Gibson JR. Visual response latencies in striate cortex of the macaque monkey. *J Neurophysiol* 68: 1332–1344, 1992.

Maunsell JH, Van Essen DC. Functional properties of neurons in middle temporal visual area of the macaque monkey. I. Selectivity for stimulus direction, speed, and orientation. *J Neurophysiol* 49: 1127–1147, 1983.

Movshon J, Adelson E, Gizzi M, Newsome W. The analysis of moving visual patterns. In: *Pattern Recognition Mechanisms*, edited by Chagas C, Gattass R, Gross CG. Rome: Vatican Press, 1985.

Movshon JA, Newsome WT. Visual response properties of striate cortical neurons projecting to area MT in macaque monkeys. *J Neurosci* 16: 7733–7741, 1996.

Naka KI, Rushton WA. S-potentials from luminosity units in the retina of fish (Cyprinidae). *J Physiol* 185: 587–599, 1966.

Nishimoto S, Gallant JL. A three-dimensional spatiotemporal receptive field model explains responses of area MT neurons to naturalistic movies. *J Neurosci* 31: 14551–14564, 2011.

Nover H, Anderson CH, DeAngelis GC. A logarithmic, scale-invariant representation of speed in macaque middle temporal area accounts for speed discrimination performance. *J Neurosci* 25: 10049–10060, 2005.

Perrone JA, Krauzlis RJ. Spatial integration by MT pattern neurons: a closer look at pattern-to-component effects and the role of speed tuning. *J Vis* 8: 1, 2008.

Priebe NJ, Cassanello CR, Lisberger SG. The neural representation of speed in macaque area MT/V5. *J Neurosci* 23: 5650–5661, 2003.

Priebe NJ, Lisberger SG, Movshon JA. Tuning for spatiotemporal frequency and speed in directionally selective neurons of macaque striate cortex. *J Neurosci* 26: 2941–2950, 2006.

Raiguel S, Van Hulle MM, Xiao DK, Marcar VL, Orban GA. Shape and spatial distribution of receptive fields and antagonistic motion surrounds in the middle temporal area (V5) of the macaque. *Eur J Neurosci* 7: 2064–2082, 1995.

Robson JG. Spatial and temporal contrast-sensitivity functions of the visual system. *J Opt Soc Am* 56: 1141–1142, 1966.

Rodman HR, Albright TD. Single-unit analysis of pattern-motion selective properties in the middle temporal visual area (MT). *Exp Brain Res* 75: 53–64, 1989.

Rodman HR, Gross CG, Albright TD. Afferent basis of visual response properties in area MT of the macaque. I. Effects of striate cortex removal. *J Neurosci* 9: 2033–2050, 1989.

Rust NC, Mante V, Simoncelli EP, Movshon JA. How MT cells analyze the motion of visual patterns. *Nat Neurosci* 9: 1421–1431, 2006.

Sceniak MP, Ringach DL, Hawken MJ, Shapley R. Contrast's effect on spatial summation by macaque V1 neurons. *Nat Neurosci* 2: 733–739, 1999.

Simoncelli EP, Heeger DJ. A model of neuronal responses in visual area MT. *Vision Res* 38: 743–761, 1998.

Smith MA, Bair W, Movshon JA. Signals in macaque striate cortical neurons that support the perception of glass patterns. *J Neurosci* 22: 8334–8345, 2002.

Smith MA, Majaj NJ, Movshon JA. Dynamics of motion signaling by neurons in macaque area MT. *Nat Neurosci* 8: 220–228, 2005.

Stoner GR, Albright TD. Neural correlates of perceptual motion coherence. *Nature* 358: 412–414, 1992.

Tolhurst DJ, Walker NS, Thompson ID, Dean AF. Non-linearities of temporal summation in neurones in area 17 of the cat. *Exp Brain Res* 38: 431–435, 1980.

Zeki SM. Functional organization of a visual area in the posterior bank of the superior temporal sulcus of the rhesus monkey. *J Physiol* 236: 549–573, 1974.